Position Optimization of Measuring Points in Voltage Non-contact Measurement of AC Overhead Transmission Lines

Dongping Xiao, Yutong Xie, Huaitong Liu, Qichao Ma, Qi Zheng, and Zhanlong Zhan

State Key Laboratory of Power Transmission Equipment & and System Security
Chongqing University, Chongqing 400044, China
xiaodongping@cqu.edu.cn, 20151102059t@cqu.edu.cn, 20141102032@cqu.edu.cn, 20151113002t@cqu.edu.cn, 20161113031t@cqu.edu.cn, zhangzl@cqu.edu.cn

Abstract ─ In this paper, an innovative idea is proposed to realize the voltage non-contact measurement of AC overhead transmission lines (OTLs), which is to reversely calculate the voltage characteristic parameters by using the measured AC electric field data under OTLs. The main challenge to realize the goal is the serious ill-posedness of the inverse problem. The condition number of the observation matrix $\boldsymbol{K}$ is the main index to reflect the ill-posedness of the inverse problem. Because the matrix $\boldsymbol{K}$ is determined by the positions of OTLs and the measuring points of electric field, it is an effective but often overlooked solution to search the optimal positions of measuring points. In this paper, an improved particle swarm optimization algorithm with the adaptive adjustment of inertia weight is developed to search the optimal measuring positions. The presented examples indicate that the selection of optimal positions for the measuring points significantly improves the accuracy and stability of the inverse solution. Meanwhile, the strong searching ability, fast convergence rate, and high stability of the proposed optimal algorithm are demonstrated as well.

Index Terms ─ AC overhead transmission lines (OTLs), electric field, ill-posed problem, inverse calculation, position optimization, voltage.

I. INTRODUCTION

The amplitude and phase of the sinusoidal voltage directly reflect the running status and health level of the AC overhead transmission lines (OTLs). Measuring the voltage of OTLs is the basis to evaluate power quality, and to diagnose and locate faults. The voltage is traditionally measured by potential transformer in the substation located at the beginning and end of OTLs. At present, the development of smart grids has increased the demand for the real-time monitoring of the OTLs' voltage to realize intelligent warning and automatic control [1, 2]. In view of the operating principle and electrical characteristics of potential transformer [3, 4], adding new potential transformers in existing lines will be confronted with many difficulties, and even it is not feasible. Therefore, some new methods of monitoring the voltage of OTLs, at the same time to meet the demands of safety and convenience, are of great value to be developed.

Numerous studies on the electromagnetic environment of high-voltage AC OTLs reveal that the power-frequency voltages of OTLs generate power-frequency electric fields in the surrounding space, which means that the sources and the fields are significantly correlated [5-8]. Thus, we propose the innovative idea to reversely calculate the voltage characteristic parameters of AC OTLs on the basis of the electric field data measured by the sensors placed under OTLs. In this way, the voltage non-contact measurement of AC OTLs can be realized.

However, the inverse calculation is a serious ill-posed problem. Specifically, the mathematical relation between the voltage matrix $\boldsymbol{U}$ and the electric field matrix $\boldsymbol{E}$ can be expressed as the following equations:

$$\boldsymbol{E} = \boldsymbol{K}\boldsymbol{U}, \tag{1}$$

where $\boldsymbol{K}$ is the observation matrix determined by the position of OTLs and the position of electric field measuring points.

Errors and noises inevitably exist in the actual measurement. We can only obtain $\boldsymbol{E}^{\delta}$ ($\|\boldsymbol{E} - \boldsymbol{E}^{\delta}\| < \delta$). If the positions of the measuring points are selected randomly, the condition number of the matrix $\boldsymbol{K}$ (i.e., cond($\boldsymbol{K}$)) may be much large. Consequently, a small noise in $\boldsymbol{E}$ may cause the inverse solution $\boldsymbol{U}^{\delta}$ to severely deviate from the true value $\boldsymbol{U}$.

Various processing methods have been proposed to address the ill-posed problem of inverse solution [9-12]. Based on our studies, we find that choosing the optimal positions of the electric field measuring points can greatly reduce cond($\boldsymbol{K}$) and the sensitivity of the inverse calculation to measuring noise.

In this paper, the optimal positions of the measuring points are searched by using cond($\boldsymbol{K}$) as the fitness function. An improved particle swarm optimization algorithm with the adaptive adjustment of inertia weight

Submitted On: December 14, 2016
Accepted On: August 12, 2017

is developed to search optimal positions. Simulation examples with different search scopes are set up and the results are compared to verify the effectiveness of the proposed method in improving the ill-posed problem. And other favorable performances of the improved particle swarm optimization algorithm are discussed.

II. MATHEMATICAL MODEL OF POWER-FREQUENCY VOLTAGES AND ELECTRIC FIELDS OF OTLS

Under the power-frequency condition, the electric field around the high-voltage OTLs can be regarded as quasi-static field and being generated only by the voltages of OTLs. The length of OTLs is far greater than the distances between the measuring points and the conductors, so two-dimensional calculation can be adopted.

The analog line charges are set in the equivalent conductors based on the Charge Simulation Method [13, 14]. The relationship between the voltage matrix $\boldsymbol{U}$ and the analog charge matrix $\boldsymbol{\tau}$ is formulated as follows:

$$\boldsymbol{U} = \boldsymbol{P}\boldsymbol{\tau}, \tag{2}$$

where $\boldsymbol{P}$ is a N dimensional potential coefficient matrix and its elements can be calculated based on the principle of mirror image:

$$\begin{cases} p_{ii} = \dfrac{1}{2\pi\varepsilon_0}\ln\dfrac{2y_i}{R_{eq}} \\ p_{ij} = \dfrac{1}{2\pi\varepsilon_0}\ln\dfrac{L_{ij}^{'}}{L_{ij}} \quad (i \neq j) \end{cases}, \tag{3}$$

where ε_0 is the dielectric constant of air, L_{ij} is the distance between the i^{th} and j^{th} conductors, $L_{ij}^{'}$ is the distance between the i^{th} mirror conductor and the j^{th} conductor, i.e.,

$$L_{ij} = \sqrt{(x_i - x_j)^2 + (y_i - y_j)^2},$$
$$L_{ij}^{'} = \sqrt{(x_i - x_j)^2 + (y_i + y_j)^2},$$

where (x_i, y_i) and (x_j, y_j) are the coordinate positions of i^{th} and j^{th} conductors, respectively.

The electric field components $E_{x\text{-}o}$ and $E_{y\text{-}o}$ at the measuring points $o(x_o, y_o)$ are represented as:

$$\begin{cases} E_{x\_o} = \boldsymbol{G}_{x-o}\boldsymbol{\tau} \\ E_{y\_o} = \boldsymbol{G}_{y-o}\boldsymbol{\tau} \end{cases}, \tag{4}$$

where $\boldsymbol{G}_{x\text{-}o}$ and $\boldsymbol{G}_{y\text{-}o}$ are N dimensional row vectors, and their i^{th} elements are given by:

$$\begin{cases} g_{x\_oi} = \dfrac{1}{2\pi\varepsilon_0}\left(\dfrac{x_o - x_i}{L_{oi}^2} - \dfrac{x_o - x_i}{L_{oi}^{'2}}\right) \\ g_{y\_oi} = \dfrac{1}{2\pi\varepsilon_0}\left(\dfrac{y_o - y_i}{L_{oi}^2} - \dfrac{y_o + y_i}{L_{oi}^{'2}}\right) \end{cases}, \tag{5}$$

where L_{oi} is the distance between the measuring points and i^{th} conductor, $L_{oi}^{'}$ is the distance between the measuring points and the i^{th} mirror conductor.

The positions of conductors, mirror conductors and measuring points, as well as the distances between them, are shown in Fig. 1.

Finally, the equations can be formed as Eq. (1). The matrix $\boldsymbol{K}$ equals:

$$\boldsymbol{K} = \boldsymbol{G}\boldsymbol{P}^{-1}. \tag{6}$$

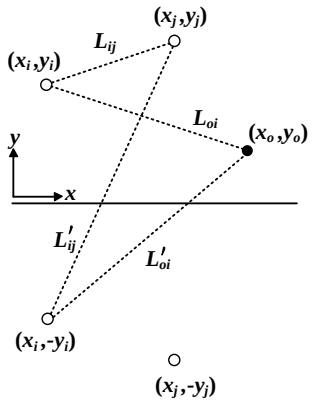

Fig. 1. Positions of the conductors, mirror conductors, measuring points and the distances between them.

III. POSITION OPTIMIZATION BASED ON IMPROVED PARTICAL SWARM OPTIMIZATION ALGORITHM

The particle swarm optimization algorithm is a global random search algorithm based on swarm intelligence. It has strong global search ability for complex problems, such as nonlinear, multi-peak, and so on. For these reasons, the particle swarm optimization algorithm has been widely applied in scientific research and engineering practice [15-18].

In the algorithm, a group of random particles should first be initialized to solve the fitness function value. Then, the location of the particle swarm should be updated, and the optimal solution is found during the successive iterations. The particle swarm updates its velocity and position by tracking the individual and global optimal positions in each iteration.

In our study, the fitness function is defined as the condition number of the matrix $\boldsymbol{K}$:

$$FitFun = \text{cond}(\boldsymbol{K}). \tag{7}$$

According to Section II, each element in $\boldsymbol{K}$ is a function with the positions of the measuring points as variables. The variables are the coordinate positions of measuring points in the x and y axes:

$$\boldsymbol{X}_m = [x_{m1}, \cdots, x_{mn}, \cdots, x_{mN}],$$
$$\boldsymbol{Y}_m = [y_{m1}, \cdots, y_{mn}, \cdots, y_{mN}],$$

where n is the order number of the measuring points, N is the number of measuring points and the dimension of the objective search space in the optimization algorithm, m is the order number of the particle, and M is the number of particles.

The goal of the optimization is to minimize *FitFun* under certain boundary conditions. That is,

$$\text{Minimize } \{FitFun\}, \tag{8}$$

subject to,

(i) $x_{\min} \le x_{mn} \le x_{\max}$ for m=1,…., M and n=1,…., N;

(ii) $y_{\min} \le y_{mn} \le y_{\max}$ for m=1,…., M and n=1,…., N.

The flight velocities of the m^{th} particle along the directions of x and y axes are, respectively,

$$\boldsymbol{V}_{x,m} = [v_{x,m1}, \cdots, v_{x,mn}, \cdots, v_{x,mN}],$$
$$\boldsymbol{V}_{y,m} = [v_{y,m1}, \cdots, v_{y,mn}, \cdots, v_{y,mN}].$$

The flight velocities of the particles affect the algorithm's searching ability. A high velocity may cause the particles to miss the optimal positions. By contrast, a slow velocity will lead to a large time cost.

During the iterative process of searching for the optimal solution, the fitness function values of each particle must be calculated and compared. Then, the historical optimal solution location of each particle $\boldsymbol{X}_{Hbest,m}$, $\boldsymbol{Y}_{Hbest,m}$ and the global history optimal solution location of the particle swarm $\boldsymbol{X}_{Gbest}$, $\boldsymbol{Y}_{Gbest}$ are dynamically updated. Finally, the particle swarm converges to the global optimal position. According to the algorithm proposed by [19], the iteration formula for the velocity and position of the particle swarm in the $(t+1)^{\text{th}}$ generation are as follows:

$$\begin{aligned}\boldsymbol{V}_{x,m}^{t+1} = {} & \omega \boldsymbol{V}_{x,m}^{t} + c_1 r_{x1}^{t+1}(X_{Hbest,m} - \boldsymbol{X}_m^t) \\ & + c_2 r_{x2}^{t+1}(X_{Gbest} - \boldsymbol{X}_m^t),\end{aligned} \tag{9a}$$

$$\begin{aligned}\boldsymbol{V}_{y,m}^{t+1} = {} & \omega \boldsymbol{V}_{y,m}^{t} + c_1 r_{y1}^{t+1}(Y_{Hbest,m} - \boldsymbol{Y}_m^t) \\ & + c_2 r_{y2}^{t+1}(Y_{Gbest} - \boldsymbol{Y}_m^t),\end{aligned} \tag{9b}$$

$$\boldsymbol{X}_m^{t+1} = \boldsymbol{X}_m^t + \boldsymbol{V}_{x,m}^{t+1}, \tag{10a}$$

$$\boldsymbol{Y}_m^{t+1} = \boldsymbol{Y}_m^t + \boldsymbol{V}_{y,m}^{t+1}, \tag{10b}$$

where ω is the inertia weight; c_1 and c_2 are the learning factors; r_{x1}^{t+1}, r_{x2}^{t+1}, r_{y1}^{t+1}, and r_{y2}^{t+1} are random numbers of the (0, 1) distribution.

The iterative termination conditions are set as reaching the maximum number of iterations and the preset fitness threshold value. Then, the optimal value of the global fitness G_{best} and its corresponding optimal positions $\boldsymbol{X}_{Gbest}$, $\boldsymbol{Y}_{Gbest}$ are output.

The inertia weight ω is one of the important parameters in the particle swarm optimization algorithm. A large ω improves the global search capability of the algorithm, whereas a small ω enhances the local search capability of the algorithm. Selecting a suitable value can balance the convergence speed and the accuracy of the algorithm. To ensure the high probability that the particles are close to the global optimal solution in the early search and are close to local optimal solution in the late search, an adaptive adjustment strategy to set the inertia weight is used to control the search process in this paper. The inertia weight ω^t used in the t^{th} iteration is determined by the following equation:

$$\omega^t = (\omega^{\text{ini}} - \omega^{\text{end}}) \times \left(\frac{t^{\text{end}} - t}{t^{\text{end}}} \right)^2 + \omega^{\text{end}}, \tag{11}$$

where ω^{ini} and ω^{end} are the initial and final values of the inertia weight, respectively; t^{end} is the total number of iterations; and t is the current iteration number.

The algorithm flow chart is shown in Fig. 2.

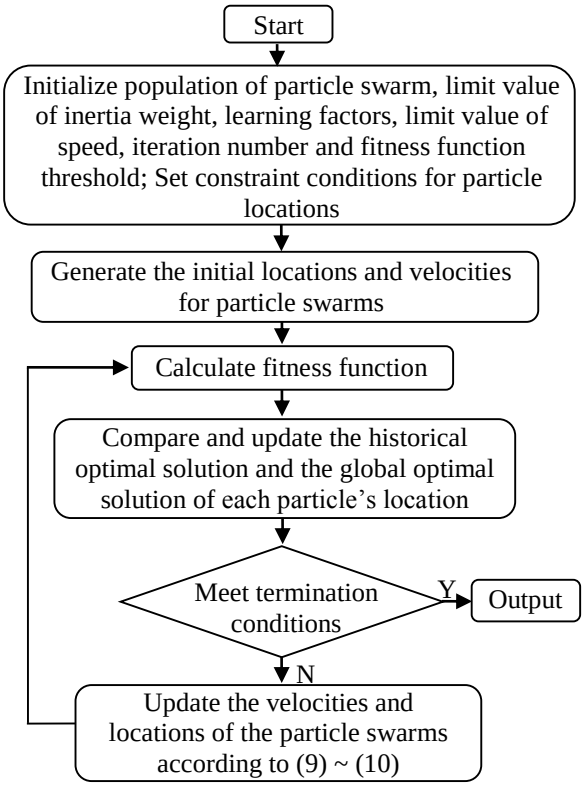

Fig. 2. Flow chart of improved particle swarm optimization algorithm.

IV. SIMULATION DETAILS AND RESULTS

A. OTLs layout and analysis condition setting

Figure 3 shows the layout of the three-phase conductors in a 220 kV OTLs system. The type of the phase conductor is 2×LGJ-400/35. The radius of the sub-conductor is 13.41 mm. The radius of the bundled circle is 0.35 m.

The analysis conditions are set as follows:

(i) The three-phase voltages of OTLs are symmetrical, i.e.,

$$\boldsymbol{U} = \begin{bmatrix} U_A \\ U_B \\ U_C \end{bmatrix} = \begin{bmatrix} 127.02\angle 0^\circ \\ 127.02\angle -120^\circ \\ 127.02\angle 120^\circ \end{bmatrix} \text{kV}.$$

(ii) Only three measuring points are set so that the electric field measurement can be easily operated in practical engineering application. The three measuring

points are symmetrically placed corresponding to the symmetrical structure of the three-phase conductors.

(iii) The accurate values of the electric fields can be calculated based on (2)~(5). Given that the actual measurement may be severely disturbed, a signal-to-noise ratio of 15 dB is set and a random Gauss white noise is added in the calculated electric fields. Then the analog electric field measurement data are generated.

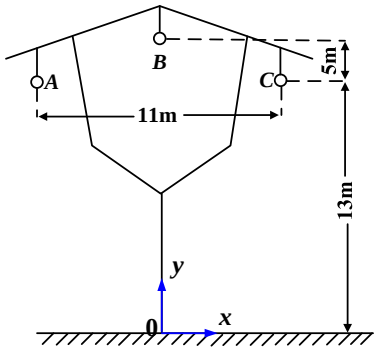

Fig. 3. Space layout of the three-phase conductors in a 220 kV OTLs system.

B. Results and analysis under the condition of randomly selecting measuring points

Three sets of measuring points are randomly selected and the corresponding cond(***K***) are calculated. The solution of voltages can be obtained by direct matrix inversion of Equation (1).

Each set of the voltages' inverse solution $\boldsymbol{U}^{\delta}$ are different because of the addition of random noise in the analog electric field measurement data. The mean and variance of $\boldsymbol{U}^{\delta}$ are calculated after running the program 10 times for each set of measuring points. The statistics are shown in Table 1.

As shown in Table 1, cond(***K***) and $\boldsymbol{U}^{\delta}$ have significant difference respectively for the three sets of measuring points that are randomly selected. The greater cond(***K***) is, the farther the inverse solution $\boldsymbol{U}^{\delta}$ deviate from the true solution ***U***. Consequently, the variances of the amplitude and angle of the calculated $\boldsymbol{U}^{\delta}$ are very large that means the stability of the inverse calculation is very poor.

C. Results and analysis under the condition of position optimization in a large space

Supposing that the optimal positions of measuring points can be searched in a large space, such as:

$$\begin{cases} -50\ \text{m} \le x_k \le 50\ \text{m} \\ 1\ \text{m} \le y_k \le 17.5\ \text{m} \end{cases}.$$

The optimal parameters are set as M=10, $\omega^{\text{ini}} = 0.9$, $\omega^{\text{end}} = 0.6$. The adaptive particle swarm optimization algorithm is used to search for the optimal positions of the measuring points with the minimum fitness function value.

Different solutions would be obtained by running program repeatedly because of the addition of random noise. Taking three sets cond(***K***) and $\boldsymbol{U}^{\delta}$ are shown in Table 2.

As shown in Table 2, although the obtained optimal positions in three optimization processes are different, the values of cond(***K***) in the three cases are approximate, which are all in the range of [1, 1.5]. Because cond(***K***) is very small, the three-phase voltages' inverse solution is close to the true value. The variance of $\boldsymbol{U}^{\delta}$ is evidently smaller than that in Table 1, which implies the computational stability is greatly improved.

Figures 4 (a)~(c) show the evolution of the global optimal solution G_{best} (i.e., the minimum of cond(***K***)) during the process of searching for the optimal positions as shown in Table 2, respectively. The three optimization processes reveal that the global optimal solution G_{best} tends to stabilize after 5~6 iterations.

Table 1: Results under the condition of randomly selecting measuring points

Measuring Points $(x_k\ y_k)$ / m	Cond(***K***)	Inverse Solution $\boldsymbol{U}^{\delta}$	
		Mean Value / kV	Variance (Amplitude Angle)
(−5.5 1.5) (0 1.5) (5.5 1.5)	98.90	199.50∠-5.8° 420.97∠−71.2° 114.77∠40.7°	(2953 1118) (19303 14603) (4998 11453)
(−7 1.5) (0 3) (7 1.5)	68.75	166.72∠5.8° 350.11∠-84.7° 146.68∠104.5°	(4335 703) (42436 14030) (3811 2309)
(−10 5) (0 5) (10 5)	20.87	128.28∠-3.5° 156.41∠-96.8° 123.18∠121.3°	(647 125) (2828 11781) (954 177)

Table 2: Results under the condition of position optimization in a large space

Measuring Points $(x_k\ y_k)$ / m	Cond($\boldsymbol{K}$)	Inverse Solution $\boldsymbol{U}^{\delta}$	
		Mean Value / kV	Variance (Amplitude Angle)
(−6.6 17.5) (0 6.8) (6.6 17.5)	1.09	$\begin{bmatrix}128.80\angle 0.5^\circ\\125.11\angle -119.9^\circ\\131.74\angle 119.3^\circ\end{bmatrix}$	(97.05 26.28) (232.67 17.32) (46.67 11.63)
(−6.1 8.4) (0 14.4) (6.1 8.4)	1.34	$\begin{bmatrix}130.41\angle 1.1^\circ\\128.72\angle -121.2^\circ\\127.21\angle 120.7^\circ\end{bmatrix}$	(102.12 39.16) (173.71 17.56) (239.56 13.92)
(−8.2 10.6) (0 14.6) (8.2 10.6)	1.36	$\begin{bmatrix}123.67\angle -2.1^\circ\\124.97\angle -117.6^\circ\\130.38\angle 120.6^\circ\end{bmatrix}$	(123.66 34.29) (124.97 19.79) (130.38 15.13)

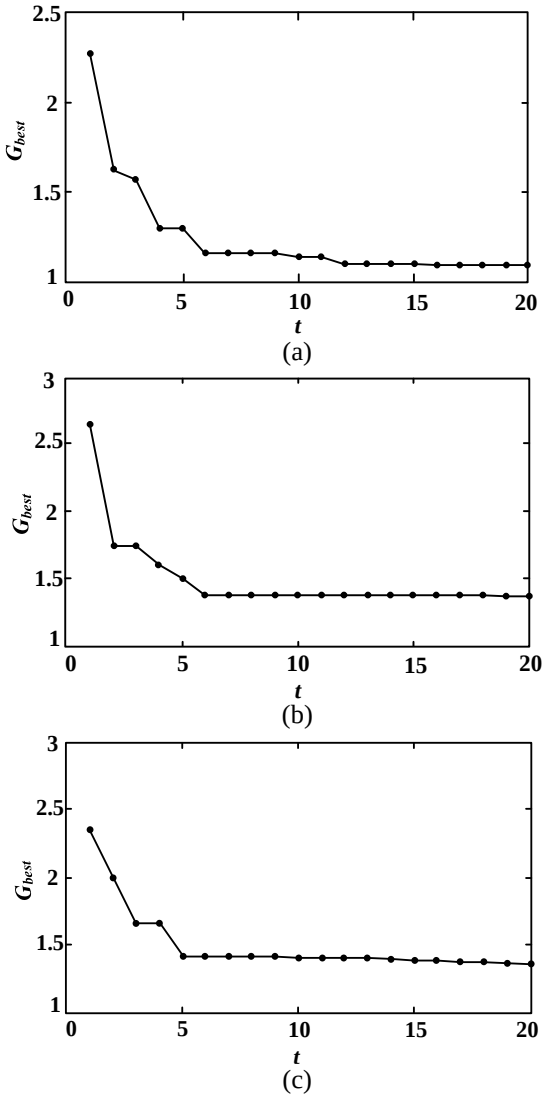

Fig. 4. Evolution of the global optimal solution G_{best} during the iterative process with adaptive adjustment ω algorithm.

D. Results and analysis under the condition of position optimization in a small space

In view of the limitations of the actual measurement conditions, the position of the measuring points can only be selected within a small space. Basing on our previous study, we propose two measurement schemes: (i) setting the measurement near the ground; (ii) setting the measurement near the conductors.

In the first measurement scheme, the search scope is set as:

$$\begin{cases}-15\ \text{m} \le x_k \le 15\ \text{m}\\ 1\ \text{m} \le y_k \le 4\ \text{m}\end{cases}.$$

The global optimal solutions obtained by separately running ten optimization processes are identical and they are (-15 4), (0 1) and (15 4). Then, cond($\boldsymbol{K}$)=21.89, and the voltage inverse solutions are:

$$\boldsymbol{U}^{\delta T} = \begin{bmatrix}143.02\angle -2.2^\circ\\148.25\angle -139.6^\circ\\114.01\angle 115.7^\circ\end{bmatrix}\text{kV}.$$

The maximum variances of the calculated amplitude and angle of the three-phase voltages are 1054 and 437, respectively.

In the second measurement scheme, the search scope is set as:

$$\begin{cases}-10\ \text{m} \le x_k \le 10\ \text{m}\\ 12\ \text{m} \le y_k \le 14\ \text{m}\end{cases}.$$

The global optimal solutions obtained by separately running ten optimization processes are also identical and they are (-9 12), (0 14) and (9 12). Then, cond($\boldsymbol{K}$)=1.46, and,

$$\boldsymbol{U}^{\delta T} = \begin{bmatrix}126.88\angle 2.2^\circ\\123.17\angle -117.2^\circ\\132.75\angle 117.4^\circ\end{bmatrix}\text{kV}.$$

The maximum variances of the calculated amplitude and angle of the three-phase voltages are 279 and 32, respectively.

The results of the position optimization process in the two measurement schemes demonstrate that the proposed algorithm can accurately search for the unique global optimal solution when the search scope is set properly.

Figures 5 (a) and 5 (b) show the comparison of the three-phase voltage waveforms in time domain between the inverse solution and the true value in the two measurement schemes, respectively.

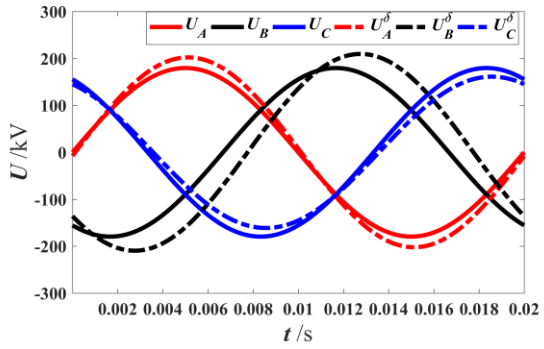

(a) In measurement scheme (i)

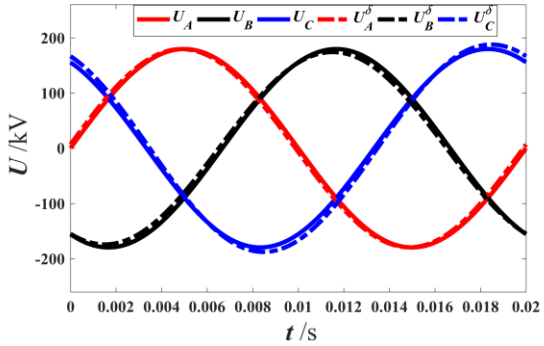

(b) In measurement scheme (ii)

Fig. 5. Comparison of the three-phase voltage waveforms in time domain between the inverse solution and the true value.

The inverse solutions obtained from the measurements near the conductors are superior to those obtained from the measurements near the ground. The error between the inverse solutions and true values is insignificant. However, measuring near the ground has the advantages of simple operation, flexibility, and safety, which is more able to reflect the superiority of the non-contact measurement approach. So further study is necessary.

V. CONCLUSION

The mathematical model between the power-frequency electric field and the voltages of OTLs is established in this paper, which reveals that it is feasible to reversely calculate the characteristic parameters of three-phase voltages by using the measured electric field data under OTLs. In view of the serious ill-posedness of the inverse solution, an improved particle swarm optimization algorithm based on adaptive adjustment of inertia weight is proposed to search for the optimal positions of the measuring points where the condition number of the observed matrix $\boldsymbol{K}$ in mathematical model is minimum. The simulation examples verify that the inverse solutions are more accurate and stable when the electric field data measured at optimal positions are used to calculate. The proposed optimization algorithm has the advantages of strong searching ability, fast convergence rate, and high stability.

Position optimization of measuring points is an effective and feasible method to weaken the ill-posedness of the specific inverse problem in this paper. It is greatly beneficial in improving the accuracy and speed of the inverse calculation. For the case that measurements are set near the ground, the regularized treatment or other inverse algorithms can be adopted further.

ACKNOWLEDGMENT

This work was supported in part by National Natural Science Foundation of China under Grant NSFC 51407016 and 51577017.

REFERENCES

[1] A. Sendin, R. Guerrero, and Pablo Angueira, "Signal injection strategies for smart metering network deployment in multitransformer secondary sub-stations," *IEEE Trans. Power Del.*, vol. 26, no. 4, pp. 2855-2861, Oct. 2011.

[2] V. M. Catterson, J. Castellon, J. A. Pilgrim, T. K. Saha, H. Ma, M. Vakilian, A. Moradnouri, M. Gholami, and B. D. Sparling, "The impact of smart grid technology on dielectrics and electrical insulation," *IEEE Trans. Dielect. El. In.*, vol. 22, no. 6, pp. 3505-3512, Jan. 2015.

[3] X. N. Lin, P. Liu, and S. M. Liu, "Ultra saturation state during transformer switch-in with load and its influence to transformer differential protection," *Proceedings of the CSEE*, vol. 22, no. 3, pp. 6-11, Mar. 2002 (in Chinese).

[4] L. X. Zhou, Z. D.Yin, and L. Zheng, "Research on principle of PT resonance in distribution power system and its suppression," *Trans. of ECS*, vol. 22, no. 5, pp. 153-158, May 2007 (in Chinese).

[5] R. G. Olsen and P. S. Wong, "Characteristics of low frequency electric and magnetic fields in the vicinity of electric power lines," *IEEE Trans. Power Del.*, vol. 7, no. 4, pp. 2046-2055, Oct. 1992.

[6] B. Florkowska, A. J. Korczynski, and M. Timler, "Analysis of electric field distribution around the high-voltage overhead transmission lines with an ADSS fiber-optic cable," *IEEE Trans. Power Del.*, vol. 19, no. 3, pp. 1183-1189, July 2004.

[7] J. H. Beggs, D. L. Marcum, and S. L. Chan, "Numerical method of characteristics for electro-

magnetics," *ACES Journal*, vol. 14, no. 2, pp. 25-36, July 1999.

[8] J. C. Salari, A. Mpalantinos, and J. I. Silva, "Comparative analysis of 2- and 3-D methods for computing electric and magnetic fields generated by overhead transmission lines," *IEEE Trans. Power Del.*, vol. 24, no. 1, pp. 338-344, Jan. 2009.

[9] A. N. Tikhonov and V. Y. Arsenin, *Solution of Ill-Posed Problems*. *Wiley*, New York, 1977.

[10] U. Hämarik and T. Raus, "On the choice of the regularization parameter in ill-posed problems with approximately given noise level of data," *J. Inv. Ill-Posed Problems*, vol. 14, no. 3, pp. 251-266, 2006.

[11] V. V. Vasin, "Relationship of several variational methods for the approximate solution of ill-posed problems," *Math. Notes. Acad. Sci. USSR*, vol. 7, no. 3, pp. 161-165, Mar. 1970.

[12] F. Yang, H. Wu, and W. He, "Investigation on the electric field inverse problem of HV transmission lines and discussion on its application," *ACES Journal*, vol. 25, no. 2, pp. 129-136, Feb. 2010.

[13] N. H. Malik, "A review of the charge simulation method and its application," *IEEE Trans. Elect. Insul.*, vol. 24, no. 1, pp. 3-20, Feb. 1989.

[14] H. Singer, H. Steinbigler, and P. Weiss, "A charge simulation method for the calculation of high voltage fields," *IEEE Trans. Power App. Syst.*, vol. 93, no. 5, pp. 1660-1668, Sep.-Oct. 1974.

[15] J. Kennedy and R. C. Eberhart, "Particle swarm optimization," *Proc. IEEE. Int. Conf. Neur. Net*., Houston, Texas, USA, pp. 1942-1948, 1995.

[16] W. C. Weng, "Optimal design of an ultra-wideband antenna with the irregular shape on radiator using particle swarm optimization," *ACES Journal*, vol. 27, no. 5, pp. 427-434, May 2012.

[17] K. E. Parsopoulos and M. N. Vrahatis, "Recent approaches to global optimization problems through particle swarm optimization," *NAT. COMPUT*, vol. 1, no. 2, pp. 235-306, June 2002.

[18] C. L. Li, C. H. Sun, C. C. Chiu, and L. F. Tuen, "Solving inverse scattering for a partially immersed metallic cylinder using steady-state genetic algorithm and asynchronous particle swarm optimization by TE waves," *ACES Journal*, vol. 28, no. 8, pp. 663-671, Aug. 2013.

[19] Y. H. Shi and R. Eberhart, "A modified particle swarm optimizer," *Proc. IEEE. Int. Conf. Evol. Comp*., Anchorage, Alaska, USA, pp. 69-73, 1998.

Dongping Xiao received the B.Sc. degree in Industrial Automation from Chongqing University, Chongqing, China, in 1999, and the M.Sc. and Ph.D. degrees in Electrical Engineering from Chongqing University, in 2004 and 2009, respectively. From 2012 to 2013, she was a Visiting Scholar with Washington State University, USA. Currently, she is an Associate Professor at the College of Electrical Engineering, Chongqing University, China. Her main fields of interests include calculation and simulation of electromagnetic field, electromagnetic measurement and running state monitoring of power transmission equipment.

Yutong Xie received the B.Eng. (Electrical Engineering) degree from Chongqing University, China, in 2015. Currently, she is studying for her master's degree (Electrical Engineering) at Chongqing University, China. Her research interest is electro-magnetic field calculation.

Huaitong Liu received the B.Eng. (Electrical Engineering) degree from Tianjin Chengjian University, China, in 2010. Currently, he is studying for his master's degree (Electrical Engineering) at Chongqing University, China. His research interests are electromagnetic field calculation and electromagnetic measurement.